
MOLECULE GRAPH NETWORKS WITH MANY-BODY EQUIVARIANT INTERACTIONS*

Zetian Mao, Jiawen Li, Chen Liang, Diptesh Das, Masato Sumita, Koji Tsuda*

Department of Computational Biology and Medical Science

The University of Tokyo

Kashiwanoha 5-1-5, Kashiwa, Chiba, 277-8561

tsuda@k.u-tokyo.ac.jp

ABSTRACT

Message passing neural networks have demonstrated significant efficacy in predicting molecular interactions. Introducing equivariant vectorial representations augments expressivity by capturing geometric data symmetries, thereby improving model accuracy. However, two-body bond vectors in opposition may cancel each other out during message passing, leading to the loss of directional information on their shared node. In this study, we develop **Equivariant N-body Interaction Networks** (ENINet) that explicitly integrates equivariant many-body interactions to preserve directional information in the message passing scheme. Experiments indicate that integrating many-body equivariant representations enhances prediction accuracy across diverse scalar and tensorial quantum chemical properties. Ablation studies show an average performance improvement of 7.9% across 11 out of 12 properties in QM9, 27.9% in forces in MD17, and 11.3% in polarizabilities (CCSD) in QM7b.

Keywords Graph neural networks, Equivariance, Molecular simulation, Tensorial property

1 Introduction

In recent years, machine learning (ML) models have shown great success in materials science by accurately predicting quantum properties of atomistic systems several orders of magnitude faster than *ab initio* simulations [1]. These ML models have practically assisted researchers in developing novel materials across various fields, such as fluorescent molecules [2], electret polymers [3] and so on.

Graph neural networks (GNNs) [4, 5] are particularly notable among ML models for atomic systems because molecules are especially suitable for 3D graph representations where each atom is characterized by its 3D Cartesian coordinate. The 3D molecular information, such as bond lengths and angles, is crucial for model learning [6, 7, 8]. However, these rotationally invariant representations may lack directional information, causing the model to view distinct structures as identical [9, 10]. When using only distances as edge features, the angle values between bond pairs are indistinguishable, which restricts the performance on angle-dependent properties, such as optical absorption [11]. Although including angle values can resolve this issue for triplet cases, a 4-atom equidistant chain with two equivalent intermediate bond angles cannot be distinguished as the middle bond rotates, resulting in a change of dihedral angles.

Equivariant architectures [12, 13] have been proposed for molecular predictions, exhibiting remarkable data efficiency by implicitly capturing the symmetries and invariances present in the data. A class of equivariant networks based on irreducible representations (*irreps*) [14, 15, 16] generates higher-order representations with spherical harmonics, achieving promising accuracy on atomic systems. Further works have enhanced these methods by introducing attention mechanisms [17, 18]. However, *irreps* suffer from intensive computations required for higher-order transformations. In contrast, equivariant vector representations can be directly obtained by processing vectors in 3D Cartesian space, achieving comparable state-of-the-art performance on various tasks with a lower computational burden [10, 19, 20].

* *Preprint*. Work in progress.

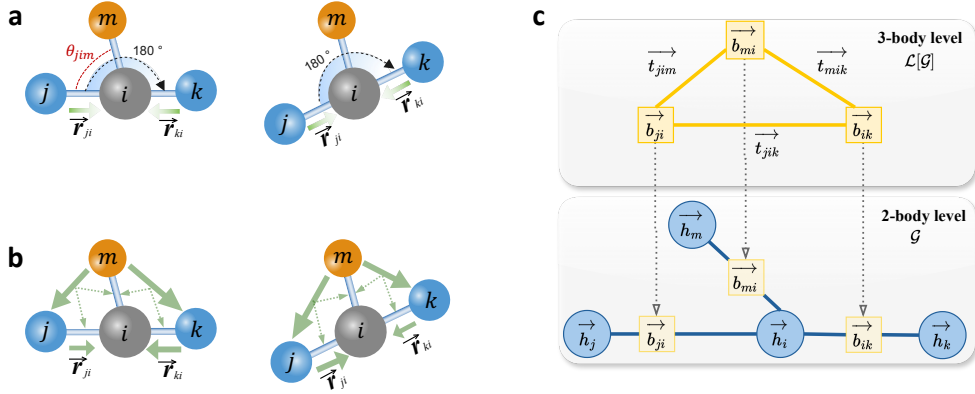


Figure 1: Example structures that cannot be distinguished with only vector features due to the vanishing of directional information aggregated onto the nodes. (a) When two equidistant bonds ji and ik are aligned in a straight line, $\vec{r}_{ji} + \vec{r}_{ki} = 0$ causes the loss of angle information among these two bonds and other bonds. Specifically, the aggregated directional information onto atom i is $\vec{r}_{ji} + \vec{r}_{ki} + \vec{r}_{mi} = \vec{r}_{mi}$ for both example structures, thus the model cannot distinguish angle changes, e.g., θ_{jim} . (b) Our approach involves integrating three-body (bond-bond) level information into bond directions to disrupt such symmetries. For instance, \vec{r}_{ji} and \vec{r}_{ki} become unsymmetrical after integrating information from \vec{r}_{mj} and \vec{r}_{mk} , so that the model can identify the two structures. (c) We achieve three-body equivariant interactions by constructing a line graph $\mathcal{L}[\mathcal{G}]$ based on the molecular graph (\mathcal{G}). Edges in $\mathcal{L}[\mathcal{G}]$ are bond-bond pairs consisting of three atoms and nodes in $\mathcal{L}[\mathcal{G}]$ are bonds that subsequently carry three-body information to the atom level in \mathcal{G} .

Equivariant directional messages are introduced between neighbor atoms, but the directional information may vanish during accumulation onto nodes as discussed in [21]. Fig. 1(a) illustrates the vanishing of directional information in bond-bond interactions when only vector features are considered. In the figure, each atom has the index within $\{i, j, k, m\}$. \vec{r}_{ji} denotes the direction vector from the atom j to atom i . θ_{jim} denotes the angle formed between the bond ji and bond im , $\theta_{jim} = \arccos \frac{\vec{r}_{ji} \cdot \vec{r}_{mi}}{\|\vec{r}_{ji}\| \cdot \|\vec{r}_{mi}\|}$. For instance, consider two neighboring atoms (j and k , shown in blue) aligned in a straight line with their common neighbor atom (i , shown in grey) within the cutoff radius. The directional vectors \vec{r}_{ji} and \vec{r}_{ki} will mutually offset, resulting in a net summation of $\vec{0}$ during message accumulation onto node i . Consequently, the model is unable to discern changes in angles formed with other bonds, such as θ_{jim} and θ_{kim} , due to the vector offset as shown by the two examples. To address this problem, Takamoto et al. included rank-2 tensor features for nodes to accumulate directional information and achieved great performance for interatomic potential [21, 22]. However, this requires extensive artificial design for the complex model architecture, making it challenging to extend the model to incorporate higher-order tensors or many-body interactions [23]. Here our work proposes to address this vectorial symmetry issue by incorporating asymmetric equivariant features convoluted at the many-body level (Fig. 1(b-c)). Incorporating many-body interactions into atoms is often necessary for enhancing interatomic potentials [24]. However, since most of these works only integrate two-body terms for constructing equivariant features, the feasibility of expressing many-body interactions with equivariant representations remains relatively unexplored. We concentrate on three-body equivariant representations for computational efficiency, but this architecture can be extended to any body level as required.

In this work, we develop **E**quivariant **N**-body **I**nteraction **N**etworks (ENINet), in which many-body level interatomic equivariant representations are constructed, while the translation invariance, rotation and reflection equivariance ($O(3)$) of outputs *w.r.t.* atomic coordinates are satisfied simultaneously. This many-body interacted architecture can be conveniently generalized to $E(3)$ equivariance (including translation, rotation and reflection equivariance) with minor modifications for specific properties.

We summarize our main contributions as follows:

- *Enhance expressivity of directional information.* We propose a new scheme to address the cancellation of bond-wise directional vectors, which may hinder the accumulation of directional information onto atoms and make certain structures indistinguishable from the model.
- *Many-body equivariance.* We achieve equivariant message passing among many-body level representations in the graph. Incorporating many-body level information, the model maintains $O(3)$ *w.r.t.* input vectors and can conveniently be converted to $E(3)$ with minor modifications.

- *Strong empirical performance.* We demonstrate the efficacy of many-body representations through benchmark molecular datasets, QM9, MD17 and QM7b polarizabilities. Our model enables the prediction of tensorial properties by incorporating equivariant features, a capability that invariant models cannot achieve. Furthermore, our approach consistently enhances accuracy across diverse molecular tasks.

2 Related Works

2.1 Many-body interactions

Accounting for many-body interactions is known to improve the accuracy of predictions [25, 26]. Several works have designed many-body descriptors that are invariant to translation, rotation, and permutations, such as the many-body tensor representation (MBTR) and others [27, 28]. With the advent of deep learning, approaches based on message passing neural networks have demonstrated superior performance on large quantum chemistry datasets [1, 29]. 3D molecular graphs are used to generate spatial many-body representations, such as angles and dihedrals, for graph learning. Most studies focus on three-body information during message interactions to maintain computational efficiency. ALIGNN [30] incorporates triplet features of atoms by constructing atomistic line graphs [31]. Similarly, CHGNet shares and updates invariant information among atom, bond and angle features [32]. M3GNet [24] computes many-body angles and integrates them into bond information for subsequent graph convolutions. DimeNet [8] jointly represents invariant distances and angles in message embedding interactions. These studies have achieved promising performance by introducing various levels of many-body representations, but the expressivity limitations of these basic invariant message passing methods have been noted [33].

2.2 Equivariant graph neural networks

Cohen et al. [34, 12] pioneered the incorporation of Euclidean equivariance into contemporary deep learning frameworks for the $SO(3)$ group. Spherical convolutional architectures with rotational equivariance were proposed for image recognition [35, 36]. The *irreps*-based methods were further applied to 3D point clouds using spherical harmonics and Clebsch-Gordan coefficients [15, 37, 14, 9], with enhancements through attention mechanisms [17, 18]. However, spherical harmonics operations are computationally intensive. Satorras et al. [38] achieved $E(n)$ equivariance within the message passing scheme, maintaining the flexibility of GNNs while ensuring computational efficiency. PaiNN [10] and TorchMD-Net [39] perform simpler equivariant interactions directly on Cartesian coordinates, demonstrating the benefits of equivariant representations for scalar targets. TeaNet [21] introduced higher-order equivariant features to mimic physical phenomena for interatomic potentials. However, the inclusion of many-body equivariant features to enhance model expressivity for molecular graph tasks is less discussed.

3 Background

3.1 Equivariance

Formally, denote the input vector space \mathcal{X} and the output vector space \mathcal{Y} . Given any transformation in a group G , the function $\mathcal{F} : \mathcal{X} \rightarrow \mathcal{Y}$ is equivariant to G if it satisfies

$$\mathcal{F} \circ D_g^{\mathcal{X}}(x) = D_g^{\mathcal{Y}} \circ \mathcal{F}(x), \forall g \in G, \forall x \in \mathcal{X} \quad (1)$$

where $D_g^{\mathcal{X}}$ and $D_g^{\mathcal{Y}}$ are the representations of the group g in the space \mathcal{X} and \mathcal{Y} , respectively [40]. Specifically, \mathcal{F} is an invariant mapping if $D_g^{\mathcal{Y}}$ corresponds to the identity operator. Therefore, invariant functions can be regarded as a special subset of equivariant functions. Equivariance is essential in molecule systems where the according transformations of vector features, *e.g.*, forces [41], dipoles [42], and higher-rank tensorial properties such as quadrupoles [43], dielectric constants [44], *w.r.t.* the system coordinates should be guaranteed.

3.2 Message passing neural networks

The message passing scheme [45, 1] unifies the prevailing GNNs into a comprehensive architecture by aggregating information in the neighborhood for each node or edge. Consider a graph $\mathcal{G} = (\mathcal{V}, \mathcal{E})$ comprising a set of nodes \mathcal{V} and edges \mathcal{E} . Each node $v_i \in \mathcal{V}$ is associated with a node feature h_i , and each edge $e_{ij} \in \mathcal{E}$ connecting the node pair v_i and v_j may optionally possess an edge feature b_{ij} . The initial features $h_i^{(0)}$ and $b_{ij}^{(0)}$ are subsequently updated through the

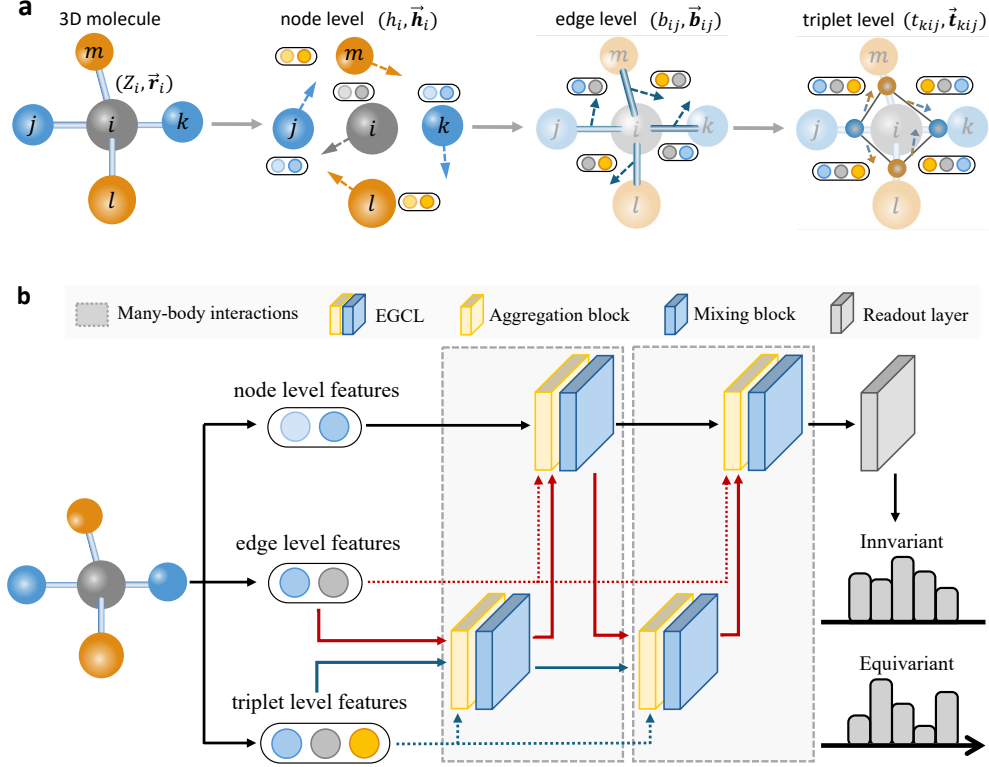


Figure 2: Schematic of the equivariant three-body interaction architecture. (a) Multi-level molecular representations. An initial 3D geometric molecule graph includes information of atomic numbers $\{Z_i\}$ and positions $\{\vec{r}_i\}$. These information is utilized to encode both invariant $\{x\}$ and equivariant features $\{\vec{x}\}$ ($x \in \{h, b, t\}$) for the node (h), edge (b) and triplet-level (t) representations, respectively. (b) Message passing scheme in ENINet. A many-body interaction block consists of two EGCLs, denoted as $\text{EGCL}(\mathcal{L}[\mathcal{G}])$ and $\text{EGCL}(\mathcal{G})$. $\text{EGCL}(\mathcal{L}[\mathcal{G}])$ integrates triplet-level features into edges. The updated edge features are subsequently passed to $\text{EGCL}(\mathcal{G})$ for message passing with the node features. As a result, each node updates its information incorporating three-body interactions. The features can be reduced through the readout layer to produce both invariant and equivariant graph-level representations.

graph convolution layers (GCL). The l -th layer GCL has the general formula,

$$m_{ij} = \phi_m(h_i^{l-1}, h_j^{l-1}, b_{ij}) \quad (2)$$

$$h_i^{(l)} = \phi_h(h_i^{l-1}, \{m_{ij}\}_{j \in \mathcal{N}(i)}) \quad (3)$$

where $\mathcal{N}(i)$ is the neighboring set of the node v_i , ϕ_m and ϕ_h are invariant learnable parameterized functions.

Equivariant graph neural networks (EGNNs) are essential for effectively processing graphs that contain geometric information, such as 3D molecular structures. The equivariant graph convolution layers (EGCL) should be able to handle directional information \vec{x}_i for each node while preserving specific equivariance properties. The incorporation of both geometric vectors and scalar features serves to enhance the model expressivity and improve task accuracy. Similarly, EGCL can be generally represented by

$$m_{ij} = \phi_m(h_i^{l-1}, h_j^{l-1}, \vec{x}_i^{l-1}, \vec{x}_j^{l-1}, b_{ij}) \quad (4)$$

$$\vec{m}_{ij} = \Phi_{\vec{m}}(h_i^{l-1}, h_j^{l-1}, \vec{x}_i^{l-1}, \vec{x}_j^{l-1}, b_{ij}) \quad (5)$$

$$h_i^{(l)} = \phi_h(h_i^{l-1}, \{m_{ij}\}_{j \in \mathcal{N}(i)}) \quad (6)$$

$$\vec{x}_i^{(l)} = \Phi_{\vec{x}}(\vec{x}_i^{l-1}, \{\vec{m}_{ij}\}_{j \in \mathcal{N}(i)}) \quad (7)$$

where $\Phi_{\vec{m}}$ and $\Phi_{\vec{x}}$ are equivariant functions *w.r.t.* corresponding input vectors. The final-layer invariant/equivariant features can be reduced to the graph-level representation.

4 Method

4.1 Molecule representations

The molecule with atoms as 3D cloud points can be represented by the geometric graph $\mathcal{G} = (\mathcal{V}, \mathcal{E})$, where the nodes are a set of $|\mathcal{V}| = N^v$ atoms and the edges are a set of $|\mathcal{E}| = N^e$ bonds. Fig. 2(a) shows the three levels of structural representations used for message passing in this work, which are originally generated from atomic numbers $\{Z_i\}^{1:N^v}$ and atom positions $\{\vec{r}_i\}^{1:N^v}$. Specifically, absolute positions generate the relative position \vec{r}_{ij} between each atom pair indexed by i, j within the cutoff range, which is separated into two components, the distance $\|\vec{r}_{ij}\|$ and the direction $\vec{r}_{ij}/\|\vec{r}_{ij}\|$.

Two types of representations, *i.e.*, invariant features and equivariant features, are assigned for each node, edge and triplet, respectively. Denote the feature dimension as d . The node set is expressed by $\mathcal{V} = \{(h_i, \vec{h}_i)\}^{1:N^v}$ where $h_i \in \mathbb{R}^{d \times 1}$ is the scalar (invariant) feature initialized with the embedding of atomic number Z_i as h_i^0 as well as other optional features such as atomic charges, and $\vec{h}_i \in \mathbb{R}^{d \times 3}$ is the vector (equivariant) feature of node i . We initialize \vec{h}_i^0 with zeros, but note that its initialization can also be the coordinate \vec{r}_i using our $E(3)$ architecture (see Appendix B) if the task depends on the starting system positions, *e.g.*, trajectory prediction of dynamic systems. Similarly, the set of edges is $\mathcal{E} = \{(b_{ij}, \vec{b}_{ij})\}^{1:N^e}$ with $b_{ij} \in \mathbb{R}^{d \times 1}$ and $\vec{b}_{ij} \in \mathbb{R}^{d \times 3}$ as bond features between the atom i and j that are converted from positional information. The Gaussian basis is applied to expand distances for b_{ij}^0 , and \vec{b}_{ij}^0 is prepared using $\vec{r}_{ij}/\|\vec{r}_{ij}\|$.

One of the main contributions of this work is the elimination of negative effects caused by the cancellation of directional information on nodes during message passing. This is achieved by augmenting equivariant interactions at the many-body level so that directional vectors can be accumulated onto node equivariant features for better expression of geometric data. To achieve this, we additionally introduce triplet features $\mathcal{T} = \{(t_{kij}, \vec{t}_{kij})\}^{1:N^t}$, where N^t is the number of triplet objects, with $t_{kij} \in \mathbb{R}^{d \times 1}$ and $\vec{t}_{kij} \in \mathbb{R}^{d \times 3}$ representing bond pairs e_{ij} and e_{ik} by constructing a line graph $\mathcal{L}[\mathcal{G}] = (\mathcal{E}, \mathcal{T})$ over the graph \mathcal{G} . The nodes \mathcal{E} in $\mathcal{L}[\mathcal{G}]$ are molecule bonds and the edges \mathcal{T} represent bond-bond interactions covering triplets of atoms. Features of edges in \mathcal{T} are simply encoded with information of two atoms at the end points of e_{ij} and e_{ik} , specifically $t_{kij}^0 = \|\vec{r}_{kj}\|$ and $\vec{t}_{kij}^0 = \vec{r}_{kj}/\|\vec{r}_{kj}\|$. By employing the features built based on triplets, ENINet can distinguish complex cases, leading to expressivity and performance enhancement as the discussion in Fig. 1.

We consider the molecular regression task in this study. Given a set of N molecules with labels $\{l_1, \dots, l_N\}$, the task is to learn inductive bias based on their graph representations $\{(\mathcal{G}_1, \mathcal{L}[\mathcal{G}]_1), \dots, (\mathcal{G}_N, \mathcal{L}[\mathcal{G}]_N)\}$ and predict the labels for the unseen molecules. The labels are either scalars or tensors equivariant to the input vectors. A summary of notations is provided in Appendix C.

4.2 Equivariant three-body interactions

The overview of ENINet architecture is visualized in Fig. 2(b). The featurizer encodes molecular graphs with three-level representations for graph convolutions. The triplet features are ultimately integrated into node features through edge features serving as the information bridge. The EGCLs for $\mathcal{L}[\mathcal{G}]$ and \mathcal{G} share the same neural network architecture. Two EGCLs, the first for the three-body level, *i.e.*, $\text{EGCL}(\mathcal{L}[\mathcal{G}])$ and the second for the two-body level, *i.e.*, $\text{EGCL}(\mathcal{G})$, form a many-body interaction block. Each EGCL comprises two steps: an aggregation step, which gathers neighbor information of nodes through message passing, and a mixing step, which updates messages between invariant and equivariant features on nodes.

In the l -th many-body interaction block, $\mathcal{L}[\mathcal{G}]$ is input into three-body $\text{EGCL}(\mathcal{L}[\mathcal{G}])$. Six features, b_{ij}^{l-1} , \vec{b}_{ij}^{l-1} , t_{kij}^{l-1} , \vec{t}_{kij}^{l-1} , $\|\vec{r}_{kj}\|$ and $\vec{r}_{kj}/\|\vec{r}_{kj}\|$ are utilized for the convolution operation. The message passing on $\mathcal{L}[\mathcal{G}]$ first integrates node and edge information to obtain new edge features:

$$t_{kij}^l = \phi_t^{\mathcal{L}[\mathcal{G}]}(b_{ij}^{l-1}, b_{ik}^{l-1}, t_{kij}^{l-1}, \|\vec{r}_{kj}\|) \quad (8)$$

$$\vec{t}_{kij}^l = \Phi_{\vec{t}}^{\mathcal{L}[\mathcal{G}]}(t_{kij}^l, \vec{b}_{ik}^{l-1}, \vec{t}_{kij}^{l-1}, \frac{\vec{r}_{kj}}{\|\vec{r}_{kj}\|}) \quad (9)$$

where all ϕ and Φ denote invariant and equivariant learnable functions, respectively. The updated edge features are aggregated into nodes, followed by normalization using the square root of the number of neighbors to stabilize training.

$$b'_{ij} = \frac{1}{\sqrt{|\mathcal{N}(i)/j|}} \sum_{k \in \mathcal{N}(i)/j} t'_{kij} \quad (10)$$

$$\vec{b}'_{ij} = \frac{1}{\sqrt{|\mathcal{N}(i)/j|}} \sum_{k \in \mathcal{N}(i)/j} \vec{t}'_{kij} \quad (11)$$

where $\mathcal{N}(i)/j$ denotes the neighboring set of the atom i except its neighbor j . Then the features are mixed between invariant and equivariant channels on nodes in $\mathcal{L}[\mathcal{G}]$.

$$\vec{b}''_{ij} = \Phi_{b'}^{\mathcal{L}[\mathcal{G}]}(b'_{ij}, \vec{b}'_{ij}, \vec{b}''_{ij}{}^{-1}) \quad (12)$$

$$b''_{ij} = \phi_{b'}^{\mathcal{L}[\mathcal{G}]}(b'_{ij}, \|\vec{b}''_{ij}\|, b''_{ij}{}^{-1}) \quad (13)$$

Up to this point, the graph convolutions in EGCL($\mathcal{L}[\mathcal{G}]$) are completed. Note that b''_{ij} and \vec{b}''_{ij} are intermediate edge features containing three-body information, serving as the inputs into the two-body EGCL. EGCL(\mathcal{G}), which shares the same neural network architecture as EGCL($\mathcal{L}[\mathcal{G}]$), performs convolutions on \mathcal{G} using six two-body inputs of h_i^{l-1} , \vec{h}_i^{l-1} , b''_{ij} , \vec{b}''_{ij} , $\|\vec{r}_{ij}\|$ and $\vec{r}_{ij}/\|\vec{r}_{ij}\|$ to produce outputs of h_i^l , \vec{h}_i^l , b^l_{ij} , \vec{b}^l_{ij} .

$$b^l_{ij} = \phi_b^{\mathcal{G}}(h_i^{l-1}, h_j^{l-1}, b''_{ij}, \|\vec{r}_{ij}\|) \quad (14)$$

$$\vec{b}^l_{ij} = \Phi_b^{\mathcal{G}}(b^l_{ij}, \vec{h}_j^{l-1}, \vec{b}''_{ij}, \frac{\vec{r}_{ij}}{\|\vec{r}_{ij}\|}) \quad (15)$$

$$h_i^l = \frac{1}{\sqrt{|\mathcal{N}(i)|}} \sum_{j \in \mathcal{N}(i)} b^l_{ij} \quad (16)$$

$$\vec{h}_i^l = \frac{1}{\sqrt{|\mathcal{N}(i)|}} \sum_{j \in \mathcal{N}(i)} \vec{b}^l_{ij} \quad (17)$$

$$\vec{h}_i^l = \Phi_h^{\mathcal{G}}(h_i^l, \vec{h}_i^l, \vec{h}_i^{l-1}) \quad (18)$$

$$h_i^l = \phi_h^{\mathcal{G}}(h_i^l, \|\vec{h}_i^l\|, h_i^{l-1}) \quad (19)$$

To this end, the information updating is completed within an entire many-body interaction block. The process does not involve absolute positions, and equivariant features are processed exclusively by equivariant operators, including linear combinations and scaling of vectors. The block achieves $O(3)$ equivariance (see detailed analysis in Appendix A). We leverage the final node representations h_i^L , \vec{h}_i^L after L many-body interaction blocks and postprocess them using the readout layer for target predictions. The extension of the architecture to encompass N -body equivariant interactions is discussed in Appendix D.

5 Experiments

We apply ENINet to three benchmark datasets, QM9 [46], MD17 [41] and dipole polarizabilities in QM7b [47]. For each task, we train two separate models, ENINet-T and ENINet-B, for ablation studies to demonstrate the expressivity enhancement achieved by additionally introducing many-body representations. ENINet-T, which includes triplet features, utilizes the full architecture as described above, while ENINet-B conducts graph convolutions only on \mathcal{G} , *i.e.*, skipping all many-body interaction EGCL($\mathcal{L}[\mathcal{G}]$)s. We enlarge the dimensionality of features in ENINet-B to ensure that the number of parameters in both models is roughly equivalent. For each experiment, we report the average results of three runs using different random seeds. The setting of hyperparameters is available in Appendix E.

5.1 QM9

The QM9 dataset is a collection of over 130k small organic molecules with DFT-calculated quantum chemical properties. The molecules contain up to 9 heavy atoms, with elements covering H, C, N, O, and F. The dataset is extensively used to train and benchmark machine learning models for predicting molecular properties. We selected a relatively more challenging data partition with fewer training samples, *i.e.*, 100k molecules for training, 18k for validation and 13k for testing, according to Cormorant [37]. The mean absolute error (MAE) between property labels and model outputs is

Table 1: The model comparison between ENINets and other models on the MAE metrics of 12 quantum chemical properties on the QM9 dataset. † denotes the model using a different train/val/test data partition. All results are taken from their original publications. The best results among all methods are underlined, and the best results from methods that use the same data partition as ours are indicated in bold.

Property Unit	α bohr ³	$\Delta\varepsilon$ meV	$\varepsilon_{\text{HOMO}}$ meV	$\varepsilon_{\text{LUMO}}$ meV	μ D	C_v cal/mol K	G meV	H meV	R^2 bohr ²	U meV	U_0 meV	ZPVE meV
NMP [†]	0.092	69	43	38	0.030	0.040	19	17	0.180	20	20	1.50
SchNet [†]	0.235	63	41	34	0.033	0.033	14	14	<u>0.073</u>	19	14	1.70
DimeNet [†]	<u>0.047</u>	<u>35</u>	28	<u>20</u>	0.029	<u>0.025</u>	9	<u>8</u>	0.331	<u>8</u>	<u>8</u>	1.29
L1Net [†]	0.088	68	46	35	0.043	0.031	14	14	0.354	14	13	1.56
Cormorant	0.085	61	34	38	0.038	0.026	20	21	0.961	21	22	2.03
LieConv	0.084	49	30	25	0.032	0.038	22	24	0.800	19	19	2.28
SEGNN	0.060	42	24	21	0.023	0.031	15	16	0.660	13	15	1.62
TFN	0.223	58	40	38	0.064	0.101	-	-	-	-	-	-
SE(3)-Tr.	0.142	53	35	33	0.051	0.054	-	-	-	-	-	-
EGNN	0.071	48	29	25	0.029	0.031	12	12	0.106	12	11	1.55
ENINet-B	0.062	49.1	28.4	23.6	0.021	0.028	9.7	8.8	0.304	9.1	8.8	1.32
ENINet-T	0.059	45.6	26.4	21.1	0.017	0.026	9.0	8.6	0.467	8.5	8.3	1.21

Table 2: The model comparison between ENINets and other models on the MAE metrics of energies (kcal/mol) and forces (kcal/mol/Å) on the MD17 dataset. Results are taken from original reports in corresponding papers. The best energy results among all methods are underlined, and the best force predictions are highlighted in bold.

Molecule		Aspirin	Ethanol	Malonaldehyde	Naphthalene	Salicylic acid	Toluene	Uracil
SchNet	<i>energy</i>	0.37	0.08	0.13	0.16	0.20	0.12	0.14
	<i>forces</i>	1.35	0.39	0.66	0.58	0.85	0.57	0.56
PhysNet	<i>energy</i>	0.230	0.059	0.094	0.142	0.126	0.100	0.108
	<i>forces</i>	0.605	0.160	0.219	0.310	0.337	0.191	0.218
DimeNet	<i>energy</i>	0.204	0.064	0.104	0.122	0.134	0.102	0.115
	<i>forces</i>	0.499	0.230	0.383	0.215	0.374	0.216	0.301
FCHL19	<i>energy</i>	0.182	<u>0.054</u>	<u>0.081</u>	0.117	0.114	0.098	0.104
	<i>forces</i>	0.478	0.136	0.245	0.151	0.221	0.203	0.105
sGDML	<i>energy</i>	0.19	0.07	0.10	0.12	0.12	0.10	0.11
	<i>forces</i>	0.68	0.33	0.41	0.11	0.28	0.14	0.24
NequIP ($l = 1$)	<i>energy</i>	-	-	-	-	-	-	-
	<i>forces</i>	0.348	0.208	0.337	0.096	0.238	0.101	0.172
PaiNN	<i>energy</i>	<u>0.159</u>	0.063	0.091	0.117	0.114	0.098	0.104
	<i>forces</i>	0.371	0.230	0.319	0.151	0.221	0.203	0.105
NewtonNet	<i>energy</i>	0.168	0.078	0.096	0.118	0.115	0.094	0.107
	<i>forces</i>	0.348	0.264	0.323	0.084	0.197	0.088	0.149
ENINet-B	<i>energy</i>	0.204	0.059	0.089	0.088	0.107	<u>0.077</u>	0.105
	<i>forces</i>	0.418	0.188	0.278	0.115	0.244	0.116	0.166
ENINet-T	<i>energy</i>	0.160	0.055	0.098	<u>0.086</u>	<u>0.106</u>	<u>0.077</u>	<u>0.089</u>
	<i>forces</i>	0.296	0.126	0.223	0.071	0.180	0.081	0.135

minimized during training. Baseline methods include NMP [1], SchNet [6], DimeNet [8], Cormorant [37], L1Net [9], LieConv [48], TFN [15], SE(3)-Tr. [17], SEGNN [49], EGNN [38]. NMP, SchNet and DimeNet are invariant models and the rest models contain equivariant features.

Table 1 presents the comparison of our results with previous works on the QM9 test set. ENINet-T achieved leading performance on eight properties ($\alpha, \mu, C_v, G, H, U, U_0, \text{ZPVE}$) in comparison with six other models that used the same data split strategy. Apart from LieConv, the remaining five models are rotationally equivariant, utilizing either *irreps* or geometric vectors. These comparisons highlight the effectiveness of our many-body equivariant representations in

Table 3: The model comparison between ENINets and AlphaML on the per-atom RMSE metrics of dipole polarizabilities (units: a.u.). The total polarizability tensor is decomposed into two irreducible components: $\lambda = 0$ and $\lambda = 2$. The values highlighted in bold and underlined represent the best performance for CCSD and DFT predictions, respectively. CCSD/DFT denotes the errors between the two computational methods for reference.

RMSE		Total	$\lambda = 0$	$\lambda = 2$
<i>CCSD/DFT(B3LYP)</i>		0.573	0.348	0.456
AlphaML	<i>CCSD</i>	0.244	0.120	0.212
	<i>DFT(B3LYP)</i>	0.302	<u>0.143</u>	0.266
ENINet-B	<i>CCSD</i>	0.247	0.170	0.179
	<i>DFT(B3LYP)</i>	0.295	0.217	0.200
ENINet-T	<i>CCSD</i>	0.219	0.158	0.152
	<i>DFT(B3LYP)</i>	<u>0.242</u>	0.165	<u>0.177</u>

enhancing performance. ENINet-T outperformed ENINet-B on all properties except R^2 , with an average performance improvement of 7.9% across these eleven improved properties.

5.2 MD17

The MD17 dataset comprises molecular dynamics simulations of small organic molecules, providing their DFT-calculated atomic trajectories. We use MD17 as a benchmark to validate the force predictions of ENINets, which are instrumental for molecular dynamics applications. With a training set of 1,000 samples, we reserve the remaining data for evaluating the accuracy of energies and forces. The model yields the scalar energy E , and its differentiation with respect to atomic positions \vec{r}_i is computed as the forces $\vec{F}_i = -\partial E / \partial \vec{r}_i$. The model is jointly trained using the energy loss and force loss with weights of 1 and 100, respectively. Furthermore, we select approaches designed for force field predictions as baseline models for comparison on MD17, including SchNet [6], PhysNet [42], DimeNet [8], FCHL19 [50], sGDML [51], NequIP [14], PaiNN [10], NewtonNet [52].

Table 2 compares the errors in energies and forces predicted by various models. It demonstrates superior accuracies compared to ENINet-B in 12 out of the 14 predictions, except for the energies of Malonaldehyde and Toluene. When compared to ENINet-B, ENINet-T exhibits an improvement of approximately 27.9% in force predictions. The advantage of equivariant features is evident as both ENINet-B and ENINet-T show significantly lower errors than invariant models such as SchNet, PhysNet, and DimeNet.

5.3 QM7b polarizabilities

Due to the incorporation of equivariant representations, ENINets can predict tensorial properties by utilizing dyadic products \otimes to produce higher-rank tensors while maintaining rotational equivariance. Following the approach [10], we employ ENINets to predict the polarizability tensor α for an n -atom system by leveraging a combination of scalar and vectorial node representations processed by gated equivariant blocks [53].

$$\alpha = \sum_{i=1}^n \left(\mathbf{I}_3(h_i) + \vec{h}_i \otimes \vec{r}_i + \vec{r}_i \otimes \vec{h}_i \right) \quad (20)$$

where \mathbf{I}_3 creates an identity, and \vec{r}_i is the position of each atom that introduces the global geometric information into the model.

We compare our method with AlphaML [54], a symmetry-adapted Gaussian process regression based scheme, by training on polarizabilities of molecules from QM7b [55, 56]. This dataset comprises 7,211 molecules containing up to seven heavy atoms including C, N, O, S and Cl. The molecular properties in the dataset were computed using linear response coupled cluster singles and doubles theory (LR-CCSD) and hybrid density functional theory (DFT), see computational details in [47]. AlphaML assesses its extrapolation capability on molecules by employing all available QM7b data to train and testing on 52 larger molecules, encompassing diverse compounds such as amino acids, nucleobases, and drug molecules. Following this data budget, we trained ENINets using a split of 6,000 molecules for training and 1,211 molecules for validation, with subsequent testing conducted on the same 52 large molecules. The accuracy of per-atom tensors was evaluated using root mean square errors (RMSE) between true values α and

predictions $\hat{\alpha}$ for N molecules, each consisting of n_i atoms.

$$\text{RMSE} \equiv \sqrt{\frac{1}{N} \sum_i \left(\frac{\|\alpha_i - \hat{\alpha}_i\|}{n_i} \right)^2} \quad (21)$$

The total polarizability tensor is decomposed into two irreducible components for error measurement: the scalar ($\lambda = 0$) $\alpha^{(0)} = \frac{\alpha_{11} + \alpha_{22} + \alpha_{33}}{\sqrt{3}}$ and the tensor ($\lambda = 2$) $\alpha^{(2)} = \sqrt{2} \left[\alpha_{12}, \alpha_{23}, \alpha_{13}, \frac{2\alpha_{33} - \alpha_{11} - \alpha_{22}}{2\sqrt{3}}, \frac{\alpha_{11} - \alpha_{22}}{2} \right]$ following [54].

Table 3 compares the performance on molecular polarizabilities. Notably, all three methods exhibit lower errors than DFT in predicting CCSD values. ENINet-T demonstrates superior performance compared to ENINet-B across all metrics, but both of them underperform AlphaML in predicting $\lambda = 0$. Specifically, ENINet-T achieves the lowest error in total RMSE for both CCSD and DFT results, showing improvements of 11.3% and 18.0% over ENINet-B, respectively. Furthermore, when predicting α_{CCSD} , it enhances accuracy by 61.8% compared to DFT errors.

6 Conclusion

In this work, we introduce many-body equivariant interactions into our model to prevent the loss of directional information during message passing. Our approach enhances model expressivity by utilizing computationally efficient equivariant representations in Cartesian space instead of spherical harmonics, achieving state-of-the-art results on benchmark datasets. The incorporation of equivariant features enables predictions of tensorial properties with rotational equivariance. Ablation studies demonstrate improved accuracy on quantum mechanism calculated properties, including energies, forces, and polarizabilities, by introducing many-body interaction layers. Additionally, the many-body equivariant method shows superior data efficiency on tasks with small training samples compared to kernel-based models known for their strong performance on small datasets, specifically FCHL19 and sGDML on MD17 forces, and AlphaML on QM7b dipole polarizabilities.

Future work. We are extending the architecture to crystal structures with periodic boundary conditions. Due to the ordered arrangement of atoms in crystal lattices, the cancellation of directional vectors in the equivariant message passing scheme is more likely to occur, making specific atomic arrangements indistinguishable. Incorporating many-body equivariant representations also has the potential to improve model performance on crystalline materials.

References

- [1] Justin Gilmer, Samuel S Schoenholz, Patrick F Riley, Oriol Vinyals, and George E Dahl. Neural message passing for quantum chemistry. In *International conference on machine learning*, pages 1263–1272. PMLR, 2017.
- [2] Masato Sumita, Kei Terayama, Naoya Suzuki, Shinsuke Ishihara, Ryo Tamura, Mandeep K Chahal, Daniel T Payne, Kazuki Yoshizoe, and Koji Tsuda. De novo creation of a naked eye-detectable fluorescent molecule based on quantum chemical computation and machine learning. *Science Advances*, 8(10):eabj3906, 2022.
- [3] Zetian Mao, Chi Chen, Yucheng Zhang, Kuniko Suzuki, and Yuji Suzuki. Ai-driven discovery of amorphous fluorinated polymer electret with improved charge stability for energy harvesting. *Advanced Materials*, page 2303827, 2023.
- [4] Thomas N Kipf and Max Welling. Semi-supervised classification with graph convolutional networks. *arXiv preprint arXiv:1609.02907*, 2016.
- [5] Keyulu Xu, Weihua Hu, Jure Leskovec, and Stefanie Jegelka. How powerful are graph neural networks? *arXiv preprint arXiv:1810.00826*, 2018.
- [6] Kristof Schütt, Pieter-Jan Kindermans, Huziel Enoc Saucedo Felix, Stefan Chmiela, Alexandre Tkatchenko, and Klaus-Robert Müller. SchNet: A continuous-filter convolutional neural network for modeling quantum interactions. *Advances in neural information processing systems*, 30, 2017.
- [7] Chi Chen, Weike Ye, Yunxing Zuo, Chen Zheng, and Shyue Ping Ong. Graph networks as a universal machine learning framework for molecules and crystals. *Chemistry of Materials*, 31(9):3564–3572, 2019.
- [8] Johannes Gasteiger, Janek Groß, and Stephan Günnemann. Directional message passing for molecular graphs. *arXiv preprint arXiv:2003.03123*, 2020.
- [9] Benjamin Kurt Miller, Mario Geiger, Tess E Smidt, and Frank Noé. Relevance of rotationally equivariant convolutions for predicting molecular properties. *arXiv preprint arXiv:2008.08461*, 2020.

- [10] Kristof Schütt, Oliver Unke, and Michael Gastegger. Equivariant message passing for the prediction of tensorial properties and molecular spectra. In *International Conference on Machine Learning*, pages 9377–9388. PMLR, 2021.
- [11] Tim Hsu, Tuan Anh Pham, Nathan Keilbart, Stephen Weitzner, James Chapman, Penghao Xiao, S Roger Qiu, Xiao Chen, and Brandon C Wood. Efficient and interpretable graph network representation for angle-dependent properties applied to optical spectroscopy. *npj Computational Materials*, 8(1):151, 2022.
- [12] Taco S Cohen and Max Welling. Steerable cnns. *arXiv preprint arXiv:1612.08498*, 2016.
- [13] Maurice Weiler, Mario Geiger, Max Welling, Wouter Boomsma, and Taco S Cohen. 3d steerable cnns: Learning rotationally equivariant features in volumetric data. *Advances in Neural Information Processing Systems*, 31, 2018.
- [14] Simon Batzner, Albert Musaelian, Lixin Sun, Mario Geiger, Jonathan P Mailoa, Mordechai Kornbluth, Nicola Molinari, Tess E Smidt, and Boris Kozinsky. E (3)-equivariant graph neural networks for data-efficient and accurate interatomic potentials. *Nature communications*, 13(1):2453, 2022.
- [15] Nathaniel Thomas, Tess Smidt, Steven Kearnes, Lusann Yang, Li Li, Kai Kohlhoff, and Patrick Riley. Tensor field networks: Rotation-and translation-equivariant neural networks for 3d point clouds. *arXiv preprint arXiv:1802.08219*, 2018.
- [16] Albert Musaelian, Simon Batzner, Anders Johansson, Lixin Sun, Cameron J Owen, Mordechai Kornbluth, and Boris Kozinsky. Learning local equivariant representations for large-scale atomistic dynamics. *Nature Communications*, 14(1):579, 2023.
- [17] Fabian Fuchs, Daniel Worrall, Volker Fischer, and Max Welling. Se (3)-transformers: 3d roto-translation equivariant attention networks. *Advances in neural information processing systems*, 33:1970–1981, 2020.
- [18] Yi-Lun Liao and Tess Smidt. Equiformer: Equivariant graph attention transformer for 3d atomistic graphs. *arXiv preprint arXiv:2206.11990*, 2022.
- [19] Stefan Doerr, Maciej Majewski, Adrià Pérez, Andreas Kramer, Cecilia Clementi, Frank Noe, Toni Giorgino, and Gianni De Fabritiis. Torchmd: A deep learning framework for molecular simulations. *Journal of chemical theory and computation*, 17(4):2355–2363, 2021.
- [20] Yu Shi, Shuxin Zheng, Guolin Ke, Yifei Shen, Jiacheng You, Jiyan He, Shengjie Luo, Chang Liu, Di He, and Tie-Yan Liu. Benchmarking graphormer on large-scale molecular modeling datasets. *arXiv preprint arXiv:2203.04810*, 2022.
- [21] So Takamoto, Satoshi Izumi, and Ju Li. Teanet: Universal neural network interatomic potential inspired by iterative electronic relaxations. *Computational Materials Science*, 207:111280, 2022.
- [22] So Takamoto, Chikashi Shinagawa, Daisuke Motoki, Kosuke Nakago, Wenwen Li, Iori Kurata, Taku Watanabe, Yoshihiro Yayama, Hiroki Iriguchi, Yusuke Asano, et al. Towards universal neural network potential for material discovery applicable to arbitrary combination of 45 elements. *Nature Communications*, 13(1):2991, 2022.
- [23] Junjie Wang, Yong Wang, Haoting Zhang, Ziyang Yang, Zhixin Liang, Jiuyang Shi, Hui-Tian Wang, Dingyu Xing, and Jian Sun. E (n)-equivariant cartesian tensor passing potential. *arXiv preprint arXiv:2402.15286*, 2024.
- [24] Chi Chen and Shyue Ping Ong. A universal graph deep learning interatomic potential for the periodic table. *Nature Computational Science*, 2(11):718–728, 2022.
- [25] Katja Hansen, Franziska Biegler, Raghunathan Ramakrishnan, Wiktor Pronobis, O Anatole Von Lilienfeld, Klaus-Robert Müller, and Alexandre Tkatchenko. Machine learning predictions of molecular properties: Accurate many-body potentials and nonlocality in chemical space. *The journal of physical chemistry letters*, 6(12):2326–2331, 2015.
- [26] Robert A DiStasio, Vivekanand V Gobre, and Alexandre Tkatchenko. Many-body van der waals interactions in molecules and condensed matter. *Journal of Physics: Condensed Matter*, 26(21):213202, 2014.
- [27] Wiktor Pronobis, Alexandre Tkatchenko, and Klaus-Robert Müller. Many-body descriptors for predicting molecular properties with machine learning: Analysis of pairwise and three-body interactions in molecules. *Journal of chemical theory and computation*, 14(6):2991–3003, 2018.
- [28] Haoyan Huo and Matthias Rupp. Unified representation of molecules and crystals for machine learning. *Machine Learning: Science and Technology*, 3(4):045017, 2022.
- [29] Kristof T Schütt, Farhad Arbabzadah, Stefan Chmiela, Klaus R Müller, and Alexandre Tkatchenko. Quantum-chemical insights from deep tensor neural networks. *Nature communications*, 8(1):13890, 2017.
- [30] Kamal Choudhary and Brian DeCost. Atomistic line graph neural network for improved materials property predictions. *npj Computational Materials*, 7(1):185, 2021.

- [31] Zhengdao Chen, Xiang Li, and Joan Bruna. Supervised community detection with line graph neural networks. *arXiv preprint arXiv:1705.08415*, 2017.
- [32] Bowen Deng, Peichen Zhong, KyuJung Jun, Janosh Riebesell, Kevin Han, Christopher J Bartel, and Gerbrand Ceder. Chgnet as a pretrained universal neural network potential for charge-informed atomistic modelling. *Nature Machine Intelligence*, 5(9):1031–1041, 2023.
- [33] Vikas Garg, Stefanie Jegelka, and Tommi Jaakkola. Generalization and representational limits of graph neural networks. In *International Conference on Machine Learning*, pages 3419–3430. PMLR, 2020.
- [34] Taco Cohen and Max Welling. Group equivariant convolutional networks. In *International conference on machine learning*, pages 2990–2999. PMLR, 2016.
- [35] Taco S Cohen, Mario Geiger, Jonas Köhler, and Max Welling. Spherical cnns. *arXiv preprint arXiv:1801.10130*, 2018.
- [36] Risi Kondor, Zhen Lin, and Shubhendu Trivedi. Clebsch–gordan nets: a fully fourier space spherical convolutional neural network. *Advances in Neural Information Processing Systems*, 31, 2018.
- [37] Brandon Anderson, Truong Son Hy, and Risi Kondor. Cormorant: Covariant molecular neural networks. *Advances in neural information processing systems*, 32, 2019.
- [38] Victor Garcia Satorras, Emiel Hoogeboom, and Max Welling. E (n) equivariant graph neural networks. In *International conference on machine learning*, pages 9323–9332. PMLR, 2021.
- [39] Philipp Thölke and Gianni De Fabritiis. Torchmd-net: Equivariant transformers for neural network based molecular potentials. *arXiv preprint arXiv:2202.02541*, 2022.
- [40] Jiaqi Han, Yu Rong, Tingyang Xu, and Wenbing Huang. Geometrically equivariant graph neural networks: A survey. *arXiv preprint arXiv:2202.07230*, 2022.
- [41] Stefan Chmiela, Alexandre Tkatchenko, Huziel E Sauceda, Igor Poltavsky, Kristof T Schütt, and Klaus-Robert Müller. Machine learning of accurate energy-conserving molecular force fields. *Science advances*, 3(5):e1603015, 2017.
- [42] Oliver T Unke and Markus Meuwly. Physnet: A neural network for predicting energies, forces, dipole moments, and partial charges. *Journal of chemical theory and computation*, 15(6):3678–3693, 2019.
- [43] Moritz Thurlmann, Lennard Bösel, and Sereina Riniker. Learning atomic multipoles: prediction of the electrostatic potential with equivariant graph neural networks. *Journal of Chemical Theory and Computation*, 18(3):1701–1710, 2022.
- [44] Zetian Mao, Wenwen Li, and Jethro Tan. Dielectric tensor prediction for inorganic materials using latent information from preferred potential. *arXiv preprint arXiv:2405.09052*, 2024.
- [45] Hanjun Dai, Bo Dai, and Le Song. Discriminative embeddings of latent variable models for structured data. In *International conference on machine learning*, pages 2702–2711. PMLR, 2016.
- [46] Raghunathan Ramakrishnan, Pavlo O Dral, Matthias Rupp, and O Anatole Von Lilienfeld. Quantum chemistry structures and properties of 134 kilo molecules. *Scientific data*, 1(1):1–7, 2014.
- [47] Yang Yang, Ka Un Lao, David M Wilkins, Andrea Grisafi, Michele Ceriotti, and Robert A DiStasio Jr. Quantum mechanical static dipole polarizabilities in the qm7b and alphaml showcase databases. *Scientific data*, 6(1):152, 2019.
- [48] Marc Finzi, Samuel Stanton, Pavel Izmailov, and Andrew Gordon Wilson. Generalizing convolutional neural networks for equivariance to lie groups on arbitrary continuous data. In *International Conference on Machine Learning*, pages 3165–3176. PMLR, 2020.
- [49] Johannes Brandstetter, Rob Hesselink, Elise van der Pol, Erik J Bekkers, and Max Welling. Geometric and physical quantities improve e (3) equivariant message passing. *arXiv preprint arXiv:2110.02905*, 2021.
- [50] Anders S Christensen, Lars A Bratholm, Felix A Faber, and O Anatole von Lilienfeld. Fchl revisited: Faster and more accurate quantum machine learning. *The Journal of chemical physics*, 152(4), 2020.
- [51] Stefan Chmiela, Huziel E Sauceda, Igor Poltavsky, Klaus-Robert Müller, and Alexandre Tkatchenko. sgdml: Constructing accurate and data efficient molecular force fields using machine learning. *Computer Physics Communications*, 240:38–45, 2019.
- [52] Mojtaba Haghghatlari, Jie Li, Xingyi Guan, Oufan Zhang, Akshaya Das, Christopher J Stein, Farnaz Heidar-Zadeh, Meili Liu, Martin Head-Gordon, Luke Bertels, et al. Newtonnet: A newtonian message passing network for deep learning of interatomic potentials and forces. *Digital Discovery*, 1(3):333–343, 2022.

- [53] Maurice Weiler, Fred A Hamprecht, and Martin Storath. Learning steerable filters for rotation equivariant cnns. In *Proceedings of the IEEE Conference on Computer Vision and Pattern Recognition*, pages 849–858, 2018.
- [54] David M Wilkins, Andrea Grisafi, Yang Yang, Ka Un Lao, Robert A DiStasio Jr, and Michele Ceriotti. Accurate molecular polarizabilities with coupled cluster theory and machine learning. *Proceedings of the National Academy of Sciences*, 116(9):3401–3406, 2019.
- [55] Lorenz C Blum and Jean-Louis Reymond. 970 million druglike small molecules for virtual screening in the chemical universe database gdb-13. *Journal of the American Chemical Society*, 131(25):8732–8733, 2009.
- [56] Grégoire Montavon, Matthias Rupp, Vivekanand Gobre, Alvaro Vazquez-Mayagoitia, Katja Hansen, Alexandre Tkatchenko, Klaus-Robert Müller, and O Anatole Von Lilienfeld. Machine learning of molecular electronic properties in chemical compound space. *New Journal of Physics*, 15(9):095003, 2013.

A Analysis on Model Equivariance

Denote the translation vector $m \in \mathbb{R}^n$ and rotation/reflection in any orthogonal matrix $Q \in \mathbb{R}^{n \times n}$ *w.r.t.* the input vectors. Any nonlinear functions approximated by multilayer perceptron (MLP) can be applied to scalar representations, but not to vector representations. Equivariant operators used in this work include linear combinations $\sum_{q=1}^p w_q \vec{x}_q$, scaling of vectors (a special case of linear combinations), and scalar products $\langle \vec{x}_1, \vec{x}_2 \rangle$ due to

$$\sum_{q=1}^p w_q (Q \vec{x}_q) = Q \sum_{q=1}^p w_q \vec{x}_q \quad (\text{A.1})$$

$$\langle Q \vec{x}_1, Q \vec{x}_2 \rangle = \vec{x}_1^\top Q^\top Q \vec{x}_2 = \vec{x}_1^\top \vec{x}_2 \quad (\text{A.2})$$

We begin by demonstrating that the graph convolutions in EGCL($\mathcal{L}[\mathcal{G}]$)s are translation invariant and rotation/reflection equivariant with respect to $\{\vec{r}_i\}$. The relative distance $\|\vec{r}_{ij}\|$ is invariant to translation, rotation, and reflection.

$$\|Q \vec{r}_i + m - (Q \vec{r}_j + m)\| = \|Q \vec{r}_{ij}\| = \sqrt{\vec{r}_{ij}^\top Q^\top Q \vec{r}_{ij}} = \sqrt{\vec{r}_{ij}^\top I \vec{r}_{ij}} = \|\vec{r}_{ij}\| \quad (\text{A.3})$$

The relative position \vec{r}_{ij} is translation invariant, but rotation and reflection equivariant to the absolute positions.

$$Q \vec{r}_i + m - (Q \vec{r}_j + m) = Q \vec{r}_i - Q \vec{r}_j = Q(\vec{r}_i - \vec{r}_j) = Q \vec{r}_{ij} \quad (\text{A.4})$$

This is the same to the unit direction vector $\vec{r}_{ij}/\|\vec{r}_{ij}\|$.

$$\frac{Q \vec{r}_i + m - (Q \vec{r}_j + m)}{\|Q \vec{r}_i + m - (Q \vec{r}_j + m)\|} = \frac{Q \vec{r}_{ij}}{\|\vec{r}_{ij}\|} = Q \frac{\vec{r}_{ij}}{\|\vec{r}_{ij}\|} \quad (\text{A.5})$$

Recall that $\vec{t}_{kij}^0 = \vec{r}_{kj}/\|\vec{r}_{kj}\|$, $\vec{b}_{ij}^0 = \vec{r}_{ij}/\|\vec{r}_{ij}\|$, $t_{kij}^0 = \|\vec{r}_{kj}\|$ and $b_{ij}^0 = \|\vec{r}_{ij}\|$. All initial inputs are invariant to absolute positions because only relative positional information is used. If we can prove that each step in EGCL($\mathcal{L}[\mathcal{G}]$) is rotation/reflection equivariant, then $O(3)$ equivariance can be guaranteed. t_{kij}^l is invariant in Eq. 8 because all the inputs $b_{ij}^{l-1}, b_{ik}^{l-1}, t_{kij}^{l-1}$ and $\|\vec{r}_{kj}\|$ are invariant as already proved. $\Phi_{\vec{t}}^{\mathcal{L}[\mathcal{G}]}$ in Eq. 9 is implemented by scaling the vectors \vec{b}_{ik}^{l-1} , \vec{t}_{kij}^{l-1} , $\vec{r}_{kj}/\|\vec{r}_{kj}\|$ with the scaling parameters that are trained using t_{kij}^l . Hence, both \vec{t}_{kij}^l and its summed features \vec{b}_{ij}^l in Eq. 11 exhibit equivariant behavior. In Eq. 12, $\Phi_{\vec{b}'}^{\mathcal{L}[\mathcal{G}]}$ is implemented using linear combinations, which is achieved by trainable linear parametric functions. Moreover, scaling is utilized based on the information learned from b_{ij}^l , applied to both \vec{b}_{ij}^l and $\vec{b}^{l-1}ij$, in order to achieve the equivariance of the output \vec{b}_{ij}^l . Up to this point, we complete illustrating the rotation/reflection equivariance and translation invariance of \vec{t}_{kij}^l and \vec{b}_{ij}^l . Any translation on $\{\vec{r}_i\}$ will not affect the outputs of EGCL($\mathcal{L}[\mathcal{G}]$).

Next, we analyze EGCL(\mathcal{G}). In this work, we set $h_i^0 = W_{Z_i} \in \mathbb{R}^{d \times 1}$ where W_{Z_i} is the element embedding vector and $\vec{h}_i^0 = \vec{0}$, without any encoded information about the absolute positions. Similar to EGCL($\mathcal{L}[\mathcal{G}]$), $\Phi_{\vec{b}}^{\mathcal{G}}$ in Eq. 15 and $\Phi_{\vec{h}}^{\mathcal{G}}$ in Eq. 18 are implemented by linear combinations and scaling of vectors. Consequently, both outputs h_i^l, \vec{h}_i^l are invariant to rotation with \vec{h}_i^l maintaining rotation and reflection equivariance since it is only processed by equivariant operations and does not include any absolute positions.

B Modification to E(3) Architecture

Our architecture is not limited to molecular graph applications. Some tasks require the model to be translation equivariant *w.r.t.* input vectors, *e.g.*, modeling N-body dynamical system in [38]. In this case, we initialize $\vec{h}_i^0 = \vec{r}_i$ to incorporate the starting position information. Assuming the scalar inputs to EGCL($\mathcal{L}[\mathcal{G}]$) do not contain any positional information and vectorial inputs only use relative positions, the outputs \vec{b}_{ij}^l remain translation invariant and rotation/reflection equivariant *w.r.t.* $\{\vec{r}_i\}$ as discussed in Appendix A. Therefore, we need to ensure that EGCL(\mathcal{G}) possesses translation equivariance.

Recall that $\Phi_{\vec{b}}^{\mathcal{G}}$ in Eq. 15 is implemented by the summation of scaled vectors.

$$\Phi_{\vec{b}}^{\mathcal{G}}(\vec{h}_j^{l-1}, \vec{b}_{ij}^l, \frac{\vec{r}_{ij}}{\|\vec{r}_{ij}\|}) = w_1 \vec{h}_j^{l-1} + w_2 \vec{b}_{ij}^l + w_3 \frac{\vec{r}_{ij}}{\|\vec{r}_{ij}\|} \quad (\text{B.6})$$

This will result in neither translation invariance nor equivariance.

$$\Phi_b^{\mathcal{G}}(Q\vec{h}_j^{l-1} + m, Q\vec{b}_{ij}^l, Q\frac{\vec{r}_{ij}}{\|\vec{r}_{ij}\|}) = w_1(Q\vec{h}_j^{l-1} + m) + w_2Q\vec{b}_{ij}^l + w_3Q\frac{\vec{r}_{ij}}{\|\vec{r}_{ij}\|} \quad (\text{B.7})$$

$$= Q(w_1\vec{h}_j^{l-1} + w_2\vec{b}_{ij}^l + w_3\frac{\vec{r}_{ij}}{\|\vec{r}_{ij}\|}) + w_1m \quad (\text{B.8})$$

$$= Q\Phi_b^{\mathcal{G}}(\vec{h}_j^{l-1}, \vec{b}_{ij}^l, \frac{\vec{r}_{ij}}{\|\vec{r}_{ij}\|}) + w_1m \quad (\text{B.9})$$

$$\neq Q\Phi_b^{\mathcal{G}}(\vec{h}_j^{l-1}, \vec{b}_{ij}^l, \frac{\vec{r}_{ij}}{\|\vec{r}_{ij}\|}) + m \quad (\text{B.10})$$

$$\neq Q\Phi_b^{\mathcal{G}}(\vec{h}_j^{l-1}, \vec{b}_{ij}^l, \frac{\vec{r}_{ij}}{\|\vec{r}_{ij}\|}) \quad (\text{B.11})$$

So we replace \vec{h}_j^{l-1} with $\vec{h}_j^{l-1} - \vec{h}_i^{l-1}$ to change Eq. 15 to

$$\vec{b}_{ij}^l = \Phi_b^{\mathcal{G}}(\vec{h}_j^{l-1} - \vec{h}_i^{l-1}, \vec{b}_{ij}^l, \frac{\vec{r}_{ij}}{\|\vec{r}_{ij}\|}) \quad (\text{B.12})$$

In this case, the translation of \vec{h} leads to the invariance of \vec{b}_{ij}^l .

$$\Phi_b^{\mathcal{G}}(Q\vec{h}_j^{l-1} + m - (Q\vec{h}_i^{l-1} + m), Q\vec{b}_{ij}^l, Q\frac{\vec{r}_{ij}}{\|\vec{r}_{ij}\|}) = w_1(Q\vec{h}_j^{l-1} + m - (Q\vec{h}_i^{l-1} + m) + w_2Q\vec{b}_{ij}^l + w_3Q\frac{\vec{r}_{ij}}{\|\vec{r}_{ij}\|} \quad (\text{B.13})$$

$$= w_1((Q\vec{h}_j^{l-1} - Q\vec{h}_i^{l-1}) + w_2Q\vec{b}_{ij}^l + w_3Q\frac{\vec{r}_{ij}}{\|\vec{r}_{ij}\|}) \quad (\text{B.14})$$

$$= Q(w_1(\vec{h}_j^{l-1} - \vec{h}_i^{l-1}) + w_2\vec{b}_{ij}^l + w_3\frac{\vec{r}_{ij}}{\|\vec{r}_{ij}\|}) \quad (\text{B.15})$$

$$= Q\Phi_b^{\mathcal{G}}(\vec{h}_j^{l-1} - \vec{h}_i^{l-1}, \vec{b}_{ij}^l, \frac{\vec{r}_{ij}}{\|\vec{r}_{ij}\|}) \quad (\text{B.16})$$

We modify Eq. 17 and Eq. 18 and combine them to achieve translation equivariance,

$$\vec{h}_i^l = \vec{h}_j^{l-1} + \frac{1}{\sqrt{|\mathcal{N}(i)|}} \sum_{j \in \mathcal{N}(i)} \vec{b}_{ij}^l \quad (\text{B.17})$$

The $E(3)$ equivariance of Eq. B.17 can be proved

$$Q\vec{h}_i^l + m = Q\left(\vec{h}_j^{l-1} + \frac{1}{\sqrt{|\mathcal{N}(i)|}} \sum_{j \in \mathcal{N}(i)} \vec{b}_{ij}^l\right) + m \quad (\text{B.18})$$

$$= \left(Q\vec{h}_j^{l-1} + \frac{1}{\sqrt{|\mathcal{N}(i)|}} \sum_{j \in \mathcal{N}(i)} Q\vec{b}_{ij}^l\right) + m \quad (\text{B.19})$$

$$= (Q\vec{h}_j^{l-1} + m) + \frac{1}{\sqrt{|\mathcal{N}(i)|}} \sum_{j \in \mathcal{N}(i)} Q\vec{b}_{ij}^l \quad (\text{B.20})$$

where the translation invariance of \vec{b}_{ij}^l has already been proved in Eq. B.12 and Eq. B.16. Therefore, \vec{h}_i^l will have the same transformation as \vec{h}_i^{l-1} . According to the above analysis, we can simply achieve the $E(3)$ equivariance using our

model by remaining $\text{EGCL}(\mathcal{L}[\mathcal{G}])$ unchanged and modifying $\text{EGCL}(\mathcal{G})$ as follows:

$$b_{ij}^l = \phi_b^{\mathcal{G}}(h_i^{l-1}, h_j^{l-1}, b_{ij}^{l-1}, \|\vec{r}_{ij}\|) \tag{B.21}$$

$$\vec{b}_{ij}^l = \Phi_b^{\mathcal{G}}(b_{ij}^l, \vec{h}_j^{l-1} - \vec{h}_i^{l-1}, \vec{b}_{ij}^{l-1}, \frac{\vec{r}_{ij}}{\|\vec{r}_{ij}\|}) \tag{B.22}$$

$$h_i^l = \frac{1}{\sqrt{|\mathcal{N}(i)|}} \sum_{j \in \mathcal{N}(i)} b_{ij}^l \tag{B.23}$$

$$\vec{h}_i^l = \frac{1}{\sqrt{|\mathcal{N}(i)|}} \sum_{j \in \mathcal{N}(i)} \vec{b}_{ij}^l + \vec{h}_i^{l-1} \tag{B.24}$$

$$h_i^l = \phi_h^{\mathcal{G}}(h_i^l, \|\vec{h}_i^l\|, h_i^{l-1}) \tag{B.25}$$

C Notations

Table C.1: Summary of notations

Notation	Description
\mathcal{G}	Graph
$\mathcal{L}[\mathcal{G}]$	Line graph
\mathcal{V}	Node set
\mathcal{E}	Edge set
\mathcal{T}	Triplet set
v_i	Node with index of i
e_{ij}	Edge between v_i and v_j
θ_{kij}	Angle formed by e_{ij} and e_{ik}
d	Feature dimension
N^v	Number of atoms
N^e	Number of bonds
N^t	Number of triplets
\vec{r}_i	Position of v_i
\vec{r}_{ij}	Relative position between \vec{r}_i and \vec{r}_j
h_i	Invariant feature of v_i
\vec{h}_i	Equivariant feature of v_i
b_{ij}	Invariant feature of e_{ij}
\vec{b}_{ij}	Equivariant feature of e_{ij}
t_{kij}	Invariant triplet feature formed by e_{ij} and e_{ik}
\vec{t}_{kij}	Equivariant triplet feature formed by e_{ij} and e_{ik}
$\mathcal{N}(i)$	Neighboring set of v_i
$\ \cdot\ $	Frobenius norm
ϕ	Parametric invariant function
Φ	Parametric equivariant function
\otimes	Dyadic product
α	Polarizability tensor

D Extension to many-body interactions

If many-body information beyond the triplet level, *e.g.*, the quadruplet, needs to be accounted for in the model, this can be achieved by simply constructing a higher-level line graph. (see Fig. D.1). For instance, consider a quadruplet in the Ethane molecule, where the nodes and edges in the graph \mathcal{G} represent atoms and bonds, respectively. We can build a line graph $\mathcal{L}[\mathcal{G}]$ based on \mathcal{G} where the nodes represent bonds and the edges represent bond-bond pairs consisting of 3 atoms. Extending this to a higher line graph $\mathcal{L}(\mathcal{L}[\mathcal{G}])$, the nodes represent bond-bond pairs and the edges represent quadruplets involving 4 atoms.

Another $\text{EGCL}(\mathcal{L}(\mathcal{L}[\mathcal{G}]))$ with the same neural network architecture as introduced in the main text can be constructed for message passing at the four-body level. Then the nodes in $\mathcal{L}(\mathcal{L}[\mathcal{G}])$, *i.e.*, triplets are input into $\text{EGCL}(\mathcal{L}[\mathcal{G}])$ to

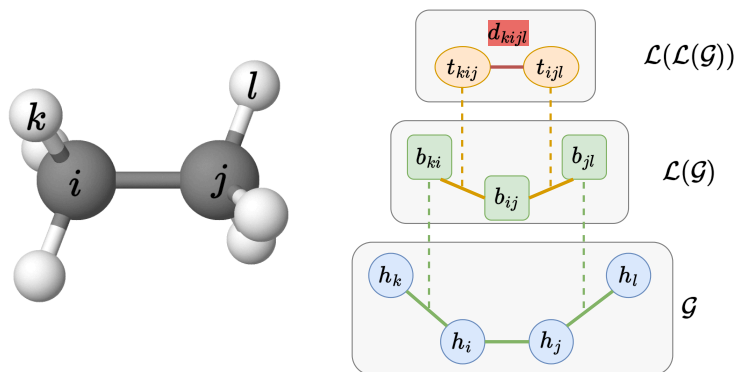


Figure D.1: Diagram of many-body representations. Higher-body level representations can be achieved by higher-level line graphs. This hierarchical approach allows for the representation of increasingly complex many-body interactions.

integrate four-body information to lower-body levels. This approach can be extended to any N -body interactions if computational cost is not a limiting factor.

E Hyperparameters

Table E.2: Summary of ENINet-T hyperparameters. Except for the feature dimension enlarged to 128, ENINet-B uses the same hyperparameters as ENINet-T. Both ENINets have around 1.22 million parameters.

Dataset	QM9	MD17	QM7b
Batch size	64	1	64
Learning rate	0.0005	0.0002	0.0005
Adam optimizer	$\beta_1 = 0.9, \beta_2 = 0.999$	$\beta_1 = 0.9, \beta_2 = 0.999$	$\beta_1 = 0.9, \beta_2 = 0.999$
# Epochs	200	200	100
Decay rate	0.6	0.8	0.5
Decay patience	10	10	10
Early stopping	50	30	50
Feature dimension	64	64	64
RBF dimension	20	20	20
# many-body interaction blocks	3	3	3
Cutoff radius (Å)	4.0	5.0	4.0
# Gated equivariant blocks	-	-	2